Biomaterials Advances 134 (2022) 112563

Contents lists available at ScienceDirect

Biomaterials Advances

journal homepage: www.elsevier.com/locate/bioadv

Using plasma-mediated covalent functionalization of rhamnolipids on polydimethylsiloxane towards the antimicrobial improvement of catheter surfaces

Maïssa Dardouri [a], Ana Bettencourt [a], Victor Martin [b,c], Filomena A. Carvalho [d], Catarina Santos [e,f], Nuno Monge [g], Nuno C. Santos [d], Maria H. Fernandes [b,c], Pedro S. Gomes [b,c,*], Isabel A.C. Ribeiro [a,**]

[a] Research Institute for Medicines (iMed.ULisboa), Faculty of Pharmacy, Universidade de Lisboa, Avenida Prof. Gama Pinto, 1649-003 Lisboa, Portugal
[b] BoneLab - Laboratory for Bone Metabolism and Regeneration – Faculty of Dental Medicine, U. Porto, Rua Dr. Manuel Pereira da Silva, 4200-393 Porto, Portugal
[c] LAQV/REQUIMTE, U. Porto, Porto 4160-007, Portugal
[d] Instituto de Medicina Molecular, Faculdade de Medicina, Universidade de Lisboa, Av. Prof. Egas Moniz, 1649-028 Lisbon, Portugal
[e] CQE, Instituto Superior Técnico, Universidade de Lisboa, Av. Rovisco Pais, 1049-001 Lisboa, Portugal
[f] EST Setúbal, CDP2T, Instituto Politécnico de Setúbal, Campus IPS, 2910 Setúbal, Portugal
[g] Centro Interdisciplinar de Estudos Educacionais (CIED), Escola Superior de Educação de Lisboa, Instituto Politécnico de Lisboa, Campus de Benfica do IPL, 1549-003 Lisboa, Portugal

ARTICLE INFO

Keywords:
Silicone
Glycolipid biosurfactants
Rhamnolipids
Medical devices
Antibiofilm
Staphylococcus aureus
Staphylococcus epidermidis

ABSTRACT

Controlling bacterial biofilm formation on silicone-based bloodstream catheters is of great concern to prevent related-infections. In this study, rhamnolipids (RLs), glycolipid biosurfactants, specifically a RLs mixture and the purified di-RL (RhaRhaC10:0C10:0) were covalently bonded to silicone with the intention of reaching long-lasting antibiofilm surfaces.

RLs mixture and di-RL were identified by an UHPLC-MS method that also allowed the confirmation of compound isolation by automated flash chromatography. Silicone surfaces underwent air-plasma treatment, inducing reactive oxygen radicals able to promote the RLs grafting that was confirmed by contact angle, FTIR-ATR and AFM measurements. The antibiofilm activity towards different Gram positive strains was evaluated by colony forming units (CFU) count and confocal laser microscopy. In addition, protein adsorption and biocompatibility were also investigated.

RLs were successfully grafted onto silicone and RLs mixture and RhaRhaC10C10:0 functionalized specimens reduced the biofilm formation over 2.3 log units against methicillin sensitive *Staphylococcus aureus*. Additionally, a decrease of 1 log unit was observed against methicillin resistant *S. aureus* and *S. epidermidis*. Functionalized samples showed cytocompatibility towards human dermal fibroblasts, hemocompatibility and no vascular irritation potential. The results mentioned above revealed a synergy between the antimicrobial and the anti-adhesive properties of RLs, making these compounds good candidates for the improvement of the medical devices antibiofilm properties.

1. Introduction

Currently, antimicrobial and antibiofilm surfaces are an emergent need to overcome bacteria colonization on medical devices and improve patients' healthcare quality [1]. This worldwide concern raised from the increasing use of medical devices through years, and hence the escalation of healthcare associated infections (HAIs). HAIs are directly related to the increase of morbidity, mortality and clinical high costs [2–4]. Among medical devices, bloodstream catheters infections, due to biofilm formation, are some of the most frequent showing a predominance of 43.4% [2]. Biofilm is a complex bacterial structure embedded in a self-produced extracellular polymeric substance, which protects pathogens from mechanical/physical stress and host-immune defenses, making them more resistant to antibiotics than when in their planktonic form [1,5,6]. Silicone such as polydimethylsiloxane (PDMS) has received a great attention in manufacturing medical stents and catheters due to its moldability, low cost, biocompatibility, good mechanical properties, topography, optic transparency, chemically inertness and gas permeability [3,7]. However, once inserted in the human body, PDMS catheters present a surface and environment prone to bacteria adherence and colonization [6,8–10]. Therefore, there is an urgent need to prevent biofilm formation on PDMS surfaces in order to avoid subsequent infections. Different strategies have been used namely antimicrobials release [11], contact killing and antiadhesive strategies. The most easy and common approach is surface coating via simple adsorption, through weak

* Correspondence to: P.S. Gomes, Faculty of Dental Medicine, U. Porto, Rua Dr. Manuel Pereira da Silva, 4200-393 Porto, Portugal.
** Correspondence to: I.A.C. Ribeiro, Faculty of Pharmacy, Universidade de Lisboa, Avenida Prof. Gama Pinto, 1649-003 Lisboa, Portugal.
E-mail addresses: pgomes@fmd.up.pt (P.S. Gomes), iribeiro@ff.ulisboa.pt (I.A.C. Ribeiro).

http://dx.doi.org/10.1016/j.msec.2021.112563
Received 19 July 2021; Received in revised form 18 October 2021; Accepted 21 November 2021
Available online 26 November 2021

interactions, allowing a fast release of active compounds [12,13]. Nevertheless, if a more long-lasting functionalization is performed via covalent bonds a more enduring activity may be obtained either acting by contact killing or antiadhesive effect. Different antimicrobials have been covalently bonded onto silicone surface and examples are, quaternary ammonium compounds [14,15], chitosan, antimicrobial peptides, enzymes and antibiotics [2,8,16]. Nevertheless, an important feature of active molecules used to avoid bacteria colonization must be the absence of development of resistance such as the one observed for antibiotics. Biosurfactants such as rhamnolipids (RLs), have gained the attention as promising molecules endowed with antiadhesive and antimicrobial activities [5,17–19]. RLs are extracellular products mainly biosynthesized by *Pseudomonas aeruginosa* and *Burkholderia* strains. They are produced as mixtures composed of one or two rhamnose molecules (hydrophilic moiety) originating mono and di-RLs respectively linked to one, two or sometimes three β-hydroxyalkanoic acids (lipidic moiety). The diversity in the RLs structures depends closely on the bacteria strain, carbon sources and the culture conditions [20].

Several studies have reported the antimicrobial properties of RLs [3,18,20–22]. However, very few studies investigated their antiadhesive activity and most of them have been performed on PDMS or polypropylene surfaces coated by adsorption with a RLs mixture showing antibiofilm activity towards Gram positive (e.g. *S. aureus*, *S. epidermidis*, *Streptococcus salivarius*) and negative bacteria (e.g. *Klebsiella pneumonia*, *Escherichia coli*, *Vibrio cholerae* and *Pseudomonas aeruginosa*) as well as yeasts (e.g. *Candida tropicalis*) [3,18,20–23]. In some industrial fields like the pharmaceutical and cosmetic, isolation and purification of compounds is needed. Thus, regarding RLs, the isolated di-RL (RhaRhaC10C10:0) that has been investigated for being one of the most abundant congener obtained from *P. aeruginosa* [22,24] may be chosen for different applications.

In the current study, a novel antimicrobial/antiadhesive approach embracing irreversible covalent functionalization of medical grade PDMS surface with a RLs mixture and the isolated RhaRhaC10C10:0 was performed. Air plasma was selected for the surface activation and APTES was used as anchor (silanization). The physicochemical modifications of the PDMS surfaces were investigated through contact angle, Fourier transform infrared-attenuated total reflectance, atomic force microscopy, as well as the antibiofilm activity and biocompatibility of obtained surfaces.

2. Materials and methods

2.1. Chemicals, reagents and materials

The following chemicals and solvents were used as received: glucose and agar from Oxoid (Hampshire, UK); potassium dihydrogen phosphate, formic acid and 2-(*N*-morpholino)ethanesulfonic acid (MES) from Merck (Darmstadt, Germany); sodium chloride from Panreac (Barcelona, Spain); (3-aminopropyl) triethoxysilane (APTES), N-(3-dimethylaminopropyl)-N′-ethylcarbodimiimide hydrochloride (EDC), N-hydroxysuccinimide (NHS), potassium chloride and sodium phosphate dibasic from Sigma-Aldrich (Saint Louis, USA); acetonitrile (pro analysis and HPLC grade) from Scharlau (Barcelona, Spain); ethanol (pro analysis) and ethyl acetate (pro analysis) from Carlo Erba (Val-de-Reuil, France), and purified water by using a Milli-Q purification system (Millipore). FDA approved medical-grade silicone (PDMS) from Sove (Portugal).

2.2. Biosurfactants

P. aeruginosa rhamnolipids were purchased from Sigma (90% purity, AGAE Technologies, Corvallis Oregon, USA).

2.3. Rhamnolipids mixture characterization and purification

Rhamnolipids mixture characterization was performed by ultra-high performanc liquid cromatography coupled to tandem mass spectrometry (UHPLC-MS/MS) according to a previously described method [25,26]. For RhaRhaC10:C10:0 isolation a flash chromatography (Teledyne Isco) automated method was performed with a reverse-phase C18 column (redisep RF 43g, Teledyne Isco) coupled to a prepacked cartridge prepared by adsorbing RLs to LiChroprep RP-18 prior to introducing into the automatic system. A gradient elution program was carried out with formic acid 0.05% aqueous solution (eluent A) and acetonitrile (eluent B). Elution started at 10% of eluent B at isocratic mode for 5 min. Successive increments of 5% of eluent B were performed respecting 5 min gradient and 5 min at isocratic until 85% of eluent B was reached. After that, 10 min of gradient to reach 100% of eluent B followed by another 10 min at isocratic 100% of eluent B. The flow rate was kept at 5 mL min^{-1} and the fractions volume at 6 mL. After identification by UHPLC-MS/MS [25], the isolated compounds were collected by mobile phase evaporation using a rotary evaporator (Buchi R-200) followed by further dryness under vacuum.

2.4. PDMS surface functionalization

2.4.1. Plasma-PDMS surface activation

Plasma technique was used in order to introduce reactive groups into PDMS surface and enhance its reactivity and wettability. The surface oxidation of PDMS samples was carried out using a plasma cleaner device (Harrick plasma, PDC-002, New York, USA) with a frequency = 50 Hz, Max power = 200 W and Max RF power = 30 W. PDMS samples were cleaned three time with distilled water for 30 min each, dried under vacuum, conducted on a glass support placed inside a chamber of 6″ Dia × 6.5″ L and submitted under high power gas-plasma for 5 min. Different gas-plasma were tested: argon (Ar), air and nitrogen (N_2) plasma.

2.4.2. RLs functionalization

2.4.2.1. 3-Aminopropyltriethoxysilane (APTES) binding. A hydrolyzed APTES solution was obtained by adding APTES to an ethanol 4% aqueous solution (V/V) adjusted to pH = 4.5 with glacial acetic acid. Plasma-treated PDMS samples were immerged directly in the APTES solution 10% (V/V) for 30 min at 50 °C and after that PDMS-APTES samples were washed 3 times with MQ water.

2.4.2.2. RLs bonding. Wet PDMS-APTES samples were directly immerged in a 0.1 M MES buffer (pH 6.0) solution containing RLs, EDC and NHS (1:3:1.5 M ratio) solution freshly prepared. The activation of the carboxylic acid end of the RLs by succinimide ester was ensured by sequential addition of EDC and NHS. EDC was allowed to react for 15 min before adding the NHS. After 60 min of reaction, a RLs solution (final concentration 1.66 or 5 mg mL^{-1}) was added and the solution remained under agitation (240 rpm, IKA® MS 3 digital) for 20 h at 25 °C. After finishing the reaction, RLs functionalized samples (PDMS-RLs) were washed 3 times with sterile MQ water and dried under vacuum atmosphere.

2.5. Surface characterization

2.5.1. Wettability

Surface wettability was conducted by contact angle measurements using a Digital Microscope (RoHS USB, China), equipped with a camera monitor and (AMCAP) software. A Milli-Q water droplet (2 μL) was deposited on the surface of vacuum-dried functionalized/non-functionalized samples at ambient humidity and temperature. The resultant angles at the droplets and substrates interface were measured using the sessile drop technique (tangent) with the Image J software (ImageJ 1.52p, National Institutes of Health, Bethesda, MD). At least four individual droplets were analyzed for each sample at 0 and 10 min after deposition. Average was obtained from at least eight independent measurements.

2.5.2. Fourier-transform infrared spectroscopy (FTIR)

Fourier Transform Infrared (FTIR) type Bruker Alpha II was used to identify the different functional groups existing on the PDMS surfaces before and after functionalization. The samples were examined in ATR

(attenuated total reflectance) mode in the range between 4000 and 800 cm^{-1} with a resolution of 4 cm^{-1}. Data acquisition and treatment were performed using OPUS 7.8 Software.

2.5.3. Atomic force microscopy

The roughness of the functionalized/non-functionalized PDMS surfaces was determined using Atomic Force Microscopy (AFM). A NanoWizard IV atomic force microscope (JPK Instruments, Berlin, Germany) mounted on the top of an Axiovert 200 inverted optical microscope (Carl Zeiss, Jena, Germany) was used for performing the scanning images of surfaces. The AFM head is equipped with a 15 μm z-range linearized piezoelectric scanner and an infrared laser. Imaging of the PDMS surfaces was performed, in air, in contact mode. Oxidized sharpened silicon pyramidal tips with a tip radius of approximately 6 nm, resonant frequency of about 190 kHz and spring constant of 58 N/m were used for the imaging. Imaging parameters were adjusted to minimize the force applied on the scanning of the topography of the PDMS surfaces. Scanning speed was optimized to 0.3 Hz and acquisition points were 512 × 512. Imaging data were analyzed with the JPK image processing v. 6.0.55 (JPK Instruments, Berlin, Germany). The average roughness (R_a) and the root mean square (RMS) roughness (R_q) of each imaged PDMS surface were quantified using same software [27–29].

2.5.4. Protein adsorption

The Bradford reagent (Biorad) protocol with bovine serum albumin (BSA, Sigma) was used for protein adsorption evaluation [30]. Each sample (functionalized and non-functionalized) was placed in a well of a 24-well microtiter plate (MTP) and added of 500 μL of BSA (1 mg mL^{-1}) in NaCl 0.9% aqueous solution. After agitation at 240 rpm (IKA® MS 3 digital) and incubation at 37 °C (Revco Ultima) for 1 h, test solutions were diluted (1:2) and 10 μL of each were added to 200 μL of Bradford reagent diluted with sterilized MiliQ water (1:4) in a 96-well MTP. The microtiter plate was then incubated at room temperature for 10 min, under agitation (120 rpm, IKA® MS 3 digital) and absorbance was measured at 595 nm in a Microplate Multimode Reader (Anthos, Zenyth 3100). A calibration curve with different BSA solutions (concentrations ranging from 0.05 to 0.6 mg mL^{-1}) was performed in order to quantify the BSA adsorbed onto the samples surfaces.

2.6. Antibiofilm activity

2.6.1. Microorganisms

Staphylococcus aureus 25923™ and *S. epidermidis 28319*™ were obtained from the American Type Culture Collection (ATCC). The clinically isolated methicillin-resistant *S. aureus* (MRSA) was kindly donated by Dr. Luisa Jordão (Instituto Nacional de Saúde Doutor Ricardo Jorge, Portugal). Aliquots from frozen stocks at −80 °C were used to culture microorganisms on Tryptic Soy Agar (TSA, Biokar Diagnostics) plates for 24 h at 37 °C.

2.6.2. Biofilm inhibition assessment

Antibiofilm activity of PDMS-RLs samples was assessed according to Pontes et al. [31]. Briefly, few colonies from a 24 h bacteria culture were suspended in Brain Heart Infusion (BHI, Biokar Diagnostics) medium supplemented with glucose 1% (*w/V*) and adjusted to 0.5 McFarland units. Plain PDMS and PDMS-RLs functionalized samples (1 × 1 cm^2) were fixed in separated wells of a 24-well MTP and added of the final inoculum to reach 1 × 10^6 colony forming units (CFU) mL^{-1} in a final volume of 1 mL in each well. MTPs were incubated for two time points, 3 h and 24 h at 37 °C. After incubation, samples were washed twice with sterile phosphate-buffered saline solution (PBS) in order to remove loosely and non-adhered bacteria. At this point some samples proceeded for biofilm CFU counts assay while others were stained for Confocal Laser Scanning Microscopy (CLSM).

2.6.2.1. Biofilm CFUs. After washing with PBS, PDMS samples were transferred into tubes containing 1 mL of sterile NaCl 0.9% aqueous solution. Then, sonication and vigorous shaking for 4 min each was executed to remove the adhered bacteria on the PDMS surfaces. Suitable dilutions were performed and an aliquot was spread in TSA plates for viability quantification. Bacteria colonies were counted after incubation for 24 h at 37 °C and results were reported as CFU cm^{-2}. Assays were carried out at least in three independent experiments.

2.6.2.2. CLSM biofilm imaging. Observation of bacteria on biofilms was evaluated using the live/dead staining assay (Invitrogen) according to [32]. After washing, samples and controls were stained with a propidium iodide (PI) (Invitrogen, Thermo Fisher Scientific) and Syto9 (Invitrogen, Thermo Fisher Scientific) combined solution. After 15 min, the dye solution was removed, samples were washed again (0.03 M sodium citrate in NaCl 0.3 M) and fixed with 4% paraformaldehyde in PBS (pH 7.4). After washing, all samples were prepared with Prolong Gold (Invitrogen) in a glass slide and observed by confocal laser scanning microscopy (CLSM, Leica TCS SP8) and using LAS X software.

2.7. Biocompatibility assays

2.7.1. Cytocompatibility assessment – direct and indirect assays

Cytocompatibility of the developed non and functionalized-PDMS samples was assessed using human dermal fibroblasts (AG22719, Coriell Institute for Medical Research) from the 8th passage. Established cultures were expanded in α-Minimal Essential Medium (α-MEM), containing 10% fetal bovine serum (FBS), 100 IU mL^{-1} penicillin, 100 μg mL^{-1} streptomycin and 2.5 μg mL^{-1} amphotericin B (all Gibco). Cells were incubated at 37 °C, and 5% CO_2 in air. After reaching approximately 70% confluence, cells were trypsinized and sub-cultured at 10^4 cells·cm^{-2} within two experimental settings: a direct and an indirect assay for the assessment of the biological response. Within the direct assay, cells were cultured directly over the non and functionalized-PDMS samples, placed on the bottom of tissue culture plates. Within the indirect assay, cells were cultured on the bottom of tissue culture plates, and a permeable insert (Transwell 6.5 mm insert, 0.4 μm permeable membrane, Costar) containing the non and functionalized-PDMS samples, was placed into the wells, allowing the microenvironmental contact with the cells, without the direct cell-material contact. Cultures were maintained for 1 and 5 days. Material samples incubated in the same experimental conditions but in the absence of cells were used as blank controls, and cells cultured in the absence of the material samples were used as positive controls.

2.7.1.1. Metabolic activity/cell proliferation. The evaluation of the metabolic activity of the cultures established within the direct assay was determined by the MTT assay, set on the reduction of the tetrazolium dye (MTT), by the nicotinamide adenine dinucleotide phosphate (NADPH)-dependent cellular oxidoreductase of the cells. At day-1 and day-5 time-points, a 10% MTT solution (5 mg mL^{-1}, Sigma-Aldrich) was added to cultured cells and incubated for 3 h. After, the supernatant was removed and the formed crystals were dissolved with dimethyl sulfoxide. The absorbance of the solution was determined at 550 nm using a microplate reader (Synergy HT; BioTek). Assays were conducted in quintuplicates.

For the indirect characterization, the metabolic activity of the cultures was assessed using the Resazurin assay, based on the reduction of resazurin salt (7-hydroxy-3H-phenoxazine-3-one-10-oxide) to the fluorescent byproduct, resorufin, by metabolically active cells. Briefly, at the referred time-points, the inserts were removed from the wells and the medium of each well was replaced by a mixture of fresh culture medium with 10% Resazurin solution (100 μg mL^{-1}, Sigma-Aldrich) for 3 h, at 37 °C. Resorufin fluorescence was then determined using a microplate reader (Synergy HT; BioTek - excitation: 540 nm, emission: 590 nm). Assays were conducted in quintuplicates.

2.7.1.2. Cell morphology. Cell morphology was evaluated by fluorescence imaging relying on filamentous actin (F-actin) staining and nucleus counterstaining, prior to microscopic observation, in both direct and

indirect assays. Briefly, cells grown at day 1 were fixed with paraformaldehyde 3.7%, permeabilized with 0.1% Triton-X (Sigma-Aldrich) and incubated with bovine serum albumin (Sigma–Aldrich), at room temperature. F-actin was stained with phalloidin-conjugated Alexa Fluor 488 (Molecular Probes), while the nuclear counterstaining was accomplished using Hoechst 33342 (Enzo). Stained cells were imaged in a Celena S digital imaging system (Logos Biosystems). Images were treated using the ImageJ software v.1.52a.

2.7.2. Hemocompatibility assessment

The hemocompatibility evaluation of the developed non and functionalized-PDMS samples was performed through hemolysis and platelet adhesion assays. Regarding hemolysis assessment, heparinized human blood was diluted with PBS (pH 7.4) and centrifuged at 2500*g*, for 5 min, at 4 °C. After, the pellet was re-suspended in PBS to obtain an erythrocyte suspension. Then, 500 μL of the obtained suspension was added to the developed non and functionalized-PDMS samples, as well as to controls (i.e., 500 μL of distilled water, as a positive control; and 500 μL of 0.9% sodium chloride solution, as a negative control). All samples were incubated for 1 h, at 37 °C, under constant shaking. Finally, samples were centrifuged at 2500*g*, for 5 min, and the supernatants' absorbance was read using a microplate reader (Synergy HT; BioTek) at 540 nm. The experiments were performed in triplicate.

The hemolysis rate was calculated using the obtained optical density (OD) values of the samples and controls, according to the equation:

$$\text{Hemolysis Rate}\% = \frac{(\text{ODsample} - \text{ODnegative control})}{(\text{ODpositive control} - \text{ODnegative control})} \times 100$$

The platelet adhesion assay was conducted from collected anticoagulated blood. Briefly, the blood was centrifuged (225*g*, 15 min, RT) to obtain platelet rich plasma. A platelet rich fraction was pooled and the platelet concentration was adjusted to 10^8 platelets mL^{-1} in PBS, further supplemented with $CaCl_2$ (2.5 mM) and $MgCl_2$ (1.0 mM). The platelet suspension was added to the non and functionalized-PDMS samples for 1 h, at 37 °C. A glass lamella was used as a negative control. Following, non-adhered platelets were rinsed from samples and the morphological characterization of the adhered platelets was conducted by scanning electron microscopy (SEM) upon fixation in 3% glutaraldehyde, dehydration in an ascending series of ethanol: water mixtures, and treatment with hexamethyldisilazane. Micrographs were acquired in a Quanta 400 FEG ESEM/EDAX Genesis X4M scanning electron microscope. 15 representative images of each group were acquired and analyzed.

2.7.3. Irritation assessment

The vascular irritation potential of the non and functionalized-PDMS samples was assessed using the HET-CAM (hen's egg-chorioallantoic membrane) test, as previously detailed [33]. Briefly, fresh fertilized White Leghorn hen's eggs were incubated at 37 °C, within a rotating egg incubator (Octagon Advance, Brinsea). Subsequently, at day 9, the incubation was interrupted and the air sac position was determined, prior to the removal of the eggshells. Subsequently, the outer membrane of the egg was carefully detached, exposing the CAM. The developed non and functionalized-PDMS samples were placed over the CAM and the irritation reaction was observed over a period of 5 min, characterizing for vascular endpoints (i.e., vessel lysis, hemorrhage and coagulation) suggestive of irritation potential. Internal controls were established in according to ICCVAM guidelines (ICCVAM, 2010), using a NaCl 0.9% solution as negative control and 1 N NaOH solution as positive control, enclosed by a silicone ring. Images were captured during the assay using a Zeiss Stemis 305 stereo microscope, coupled with an Axiocam 5 Color Camera. Assays were conducted in quintuplicates.

2.8. Statistical analysis

For the contact angle evaluation and for the biofilm activity assays, the statistical analysis between the different samples was performed by applying the unpaired Student's *t*-test. Regarding AFM, the obtained results for PDMS-RLs surface roughness (R_a and R_q) were compared with the respective values for PDMS-APTES samples. This analysis was performed by applying paired Student's *t*-test. The statistical significance was set at p values <0.05 with a 95% confidence interval. Statistical analysis was performed using GraphPad Prism 5 software v.5.03 (GraphPad Software, San Diego, California, USA).

In biocompatibility assessment normality of the data was determined by the Shapiro-Wilk test. In which regards to normally-distributed datasets, one-way analysis of variance (ANOVA) was performed, followed by Tukey post hoc test. Regarding non-normally distributed datasets, Kruskal-Wallis test followed by multiple comparisons using Dunn's test, was performed. p values <0.05 were considered significant. Statistical analysis was performed in the IBM SPSS statistics 26.0 software.

3. Results and discussion

3.1. Characterization and purification of RLs mixture

The different components of the RLs mixture identified by UHPLC-MS/MS are shown in the Table 1. The mixture presented mono and dirhamnolipids integrating different combinations of (unsaturated or saturated) fatty acids. Only RLs mixture and the isolated RhaRhaC10:0C10:0 were used in further experiments due to their abundance as well as for their antimicrobial and antibiofilm properties previously reported [24,34,35].

3.2. Optimization of functionalization conditions

Three main steps defined the PDMS functionalization process in this work: i) gas-plasma activation of the PDMS surface; ii) APTES PDMS surface modification and iii) RLs functionalization. Two different parameters were tested for a protocol optimization: the gas used for plasma and the RLs concentration.

3.2.1. Gas-plasma optimization

PDMS substrates were subjected to Ar, air and N_2 -plasma at fixed exposure time of 5 min and fixed RLs concentration (10 mg mL^{-1}). Contact angle, FTIR-ATR spectra and the antibiofilm activity of the plain PDMS and Ar/air/N_2-PDMS-RLs samples were evaluated. PDMS hydrophobicity was confirmed as a contact angle of 108.4° at $t = 0$ min and 91.3° at $t =$ 10 min (after surface achieved equilibrium) was observed. Additionally, contact angles of 83.0°, 85.0°, 89.0° were obtained after APTES modification following Ar, air, N_2-plasma exposure, respectively. The contact angle measurements of RLs-functionalized samples are shown in Fig. 1A. A pronounced decrease in the contact angle (below 14°) for all surfaces was observed after RLs functionalization (Fig. 1A). The decrease in the contact angle measurements promoted the change from the hydrophobic to the hydrophilic character of the surface confirming the PDMS surface modification established in each functionalization step.

Moreover, Fig. 1B shows the FTIR-ATR spectra of PDMS, RLs and Ar/air/N_2-PDMS-RLs. The FTIR-ATR spectra of Ar/air/N_2-PDMS-RLs substrates retained specific bands of PDMS such as: the vibration bands at 1010 and 1100 cm^{-1} attributed to the stretching vibration of Si-O-Si bonds; the 1265 cm^{-1} band that is due to the various vibration of the CH bonds coming from the PDMS methyl groups Si-$(CH_3)_2$; and finally, the band at 2965 cm^{-1} that is characteristic of CH stretching vibrations of -CH_3 [9,35].

Two additional bands were detected at 1665 cm^{-1} and 1573 cm^{-1} which can be attributed to the stretching vibration of the amide carbonyl group and the amide I groups, respectively [9,36–38]. These two bands are related to the amide group that is formed by the covalent bond of RLs carboxylic end with the APTES amine group. Thus, these results confirm the chemical bonding of the RLs to APTES previously covalently bonded to the PDMS surfaces. In addition, all the Ar/air/N_2-PDMS-RLs showed the characteristic bands of the RLs structure such as: i) the broad band

Table 1
UHPLC-MS identification, molecular weight and structure of the main RLs congeners detected with H^+, Na^+ and K^+ adducts. (1)Rhamnolipids isomers may be present.

Rhamnolipids	MW	Adduct m/z	Rhamnolipids structure
RhaRhaC8:0C10:0:0(1)	622	$[M+H]^+$ 623	**Mono-rhamnolipids n_1, n_2= [1-9]** 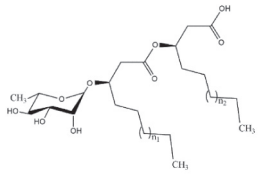
RhaC8:0C10:0:0(1)	476	$[M+H]^+$ 477	
RhaRhaC8:0C12:0(1)	650	$[M+H]^+$ 651	
RhaRhaC10:0C10:1(1)	648	$[M+K]^+$ 687	
RhaRhaC10:C12:1(1)	676	$[M+Na]^+$ 699	
RhaRhaC10:0C10:0(1)	650	$[M+H]^+$ 651	
RhaRhaC10:0C12:0(1)	678	$[M+H]^+$ 679	**Di-rhamnolipids n_1, n_2= [1-9]** 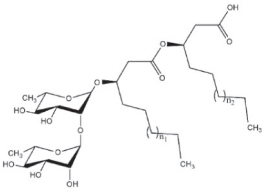
RhaC10:0C12:1(1)	530	$[M+K]^+$ 569	
RhaC10:0C10:1(1)	502	$[M+Na]^+$ 525	
RhaRhaC10:0C14:1(1)	704	$[M+Na]^+$ 727	
RhaC10:0C12:0(1)	532	$[M+H]^+$ 533	

observed at ~3380 cm^{-1} attributed to the stretching vibration of OH group from the RLs skeleton; ii) the sharp bands detected at 2931 cm^{-1} and 2860 cm^{-1} assigned, respectively, to the symmetric and asymmetric stretching vibration of the CH group [9,36,38]; iii) the carbonyl (C=O) stretching vibration band of the ester groups of the free RLs revealed at 1740 cm^{-1}. After the covalent linkage of the RLs to the PDMS surface a shift on the carbonyl vibrational band to 1709 cm^{-1} and 1700 cm^{-1} in the air-PDMS-RLs and N_2-PDMS-RLs spectra, respectively, was observed. Additionally, the bands detected at 1468 and 1408 cm^{-1} are assigned to the OH and CH_2 deformation vibrations, respectively [38]. The bands observed at 1131 cm^{-1} and 1055 cm^{-1} can be attributed to the C-O-C stretching vibrations in the rhamnose ring [38,39].

The intensity of all bands from the RLs chemical skeleton increases considerably when using the air and N_2 gas plasma for the PDMS surface activation which suggest that the chemical bonding of the RLs to the PDMS surfaces is dependent on the gases used and more effective for these two (air and N_2 gas plasma) gases when compared with Ar.

Additionally, antimicrobial assays were performed on the PDMS and Ar/air/N_2-PDMS-RLs. Log (CFU cm^{-2}) values of 4.61 ± 0.11; 4.36 ± 0.05 and 4.86 ± 0.11 were achieved for Ar, air and N_2-PDMS-RLs, respectively. The use of different activation gases led to a significantly different Log (CFU) results when comparing between them (Fig. 1A). Therefore, plasma subsequent experiments were performed with air since it generated the lowest Log (CFU) values and also for to its availability, low cost and safety.

3.2.2. Optimization of the RLs concentration

Two RLs concentrations, 1.66 ($RLs_{1.66}$) and 5 mg mL^{-1} (RLs_5) were investigated for the functionalization of PDMS surface while maintaining fixed all the other parameters (i.e., air-plasma, 5 min exposure time). Fig. 2 exhibits the antibiofilm activity of plain PDMS (Control), PDMS functionalized with APTES (APTES), PDMS functionalized with $RLs_{1.66}$ ($RLs_{1.66}$) and RLs_5 (RLs_5) against *S. aureus* ATCC *25923*. PDMS-RLs_5 showed higher anti-biofilm activity than $RLs_{1.66}$ at both end points. The Log reduction after 3 h of incubation was 0.75 and 1.62 and after 24 h was 1.47 and 2.4 for $RLs_{1.66}$ and RLs_5, respectively. Therefore, and according to the statistical results, the RLs concentration selected for further experiments was fixed at 5 mg mL^{-1} since there was no considerable difference in the biofilm formation when using a concentration of 10 mg mL^{-1} under the same experimental conditions (Log = 4.36 ± 0.05 ≈ 4.37 ± 0.08, Figs. 1A and 2A).

3.3. Functionalization of PDMS with RLs mixture and RhaRhaC10C10:0

3.3.1. Surface characterization

3.3.1.1. Contact angle. Considering the importance of knowing the surface wettability properties of PDMS after APTES, RLs mixture (RLs mix) and RhaRhaC10C10:0 (di-RL) surface functionalization, contact angle (CA) measurements were performed (Fig. 3). The PDMS presented a hydrophobic surface (CA = 91.3 ± 2.2°) after 10 min, when water surface reaches equilibrium, while after APTES, RLs mix and di-RL functionalization, the contact angle decreased to 78.2 ± 5.0°, 23.9 ± 3.3° and 9.82 ± 1.0°, respectively. Hence, the enhancement of the hydrophilic character of the analyzed surfaces confirms the PDMS surface functionalization. This can be due to the presence of polar reactive groups on the PDMS surface such as -NH_2 coming from the silanization of the PDMS surface after APTES functionalization, -OH and ester groups coming from the plasma treatment and the RLs functionalization [9], suggesting that the plasma-assisted and chemical functionalization with APTES, RLs mix and di-RL were properly performed and improved the hydrophilic character of the PDMS surfaces. Results were in accordance with those of Hajfarajollah et al. [40] which revealed changes on wettability surface properties with a decrease on the contact angle value from 91.3 ± 2.3° to 12.2 ± 1.4° after RLs adsorption onto a polypropylene surface previously treated with air-plasma. Another important factor that can have a strong impact on the wettability of the surfaces is the surface roughness induced by the functionalization [41]. In order to investigate the effect of functionalization on the PDMS surfaces, AFM analysis were performed.

3.3.1.2. Atomic force microscopy. Fig. 4 shows the 3-dimensional AFM scanning height images where it is possible to compare the differences between the PDMS surface after air treatment, functionalization with APTES (only) and functionalization with RLs (in mixture and isolated).

Air plasma treatment and silanization with APTES turned PDMS surface slightly smoother (p = 0.0053 for R_a and p = 0.010 for R_q), as already shown by other authors [42].

On the contrary, the RLs addition to the PDMS surface either with the isolated RhaRhaC10C10 (di-RL) or RLs mixture (RLs mix) increased the roughness of the surface, more significantly for the later one (Fig. 4A and B). The increase in the roughness of the PDMS in the presence

A

Samples	Contact Angle (°)	Log CFU cm^{-2}
Ar-PDMS-RLs	13.5 ± 0.19	4.61 ± 0.11 [a]
Air-PDMS-RLs	12.14 ± 0.52	4.36 ± 0.05 [b]
N_2-PDMS-RLs	9.80 ± 0.94	4.86 ± 0.11 [c]

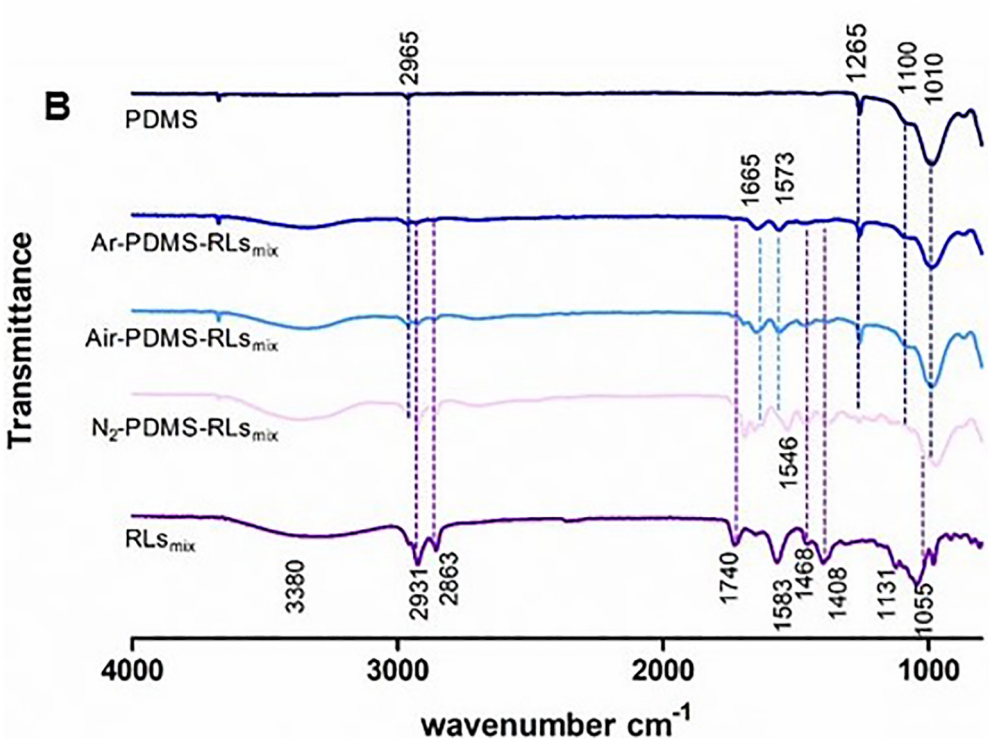

Fig. 1. A. Contact angle measurements (t = 10 min) and antibiofilm activity after 3 h of incubation (expressed as Log (CFU cm^{-2})). Data are shown as mean values ± standard deviation (SD). Statistical parameters with respect to antibiofilm results: a ≠ b ($p < 0.01$), b ≠ c ($p < 0.001$), a ≠ c ($p < 0.05$). B. FTIR-ATR spectra of bare PDMS, functionalized PDMS when using different gas sources (Ar-PDMS-RLs, Air-PDMS-RLs, N_2-PDMS-RLs) and RLs mixture.

of RLs (isolated or in mixture) confirms that the functionalization with RLs was successful. The results suggest a surface restructuring with the bonding of the compounds. In the case of the RLs mixture distinctive compounds (mono and di-RLs) were linked to the surface leading to a higher restructuring of the surface and an increase in surface RMS roughness (p = 0.0326 for the comparison between RLs mix and di- RL).

Data suggest that the addition of the compounds to the PDMS surface increased its roughness due to its non-homogenous binding through the PDMS-APTES surface.

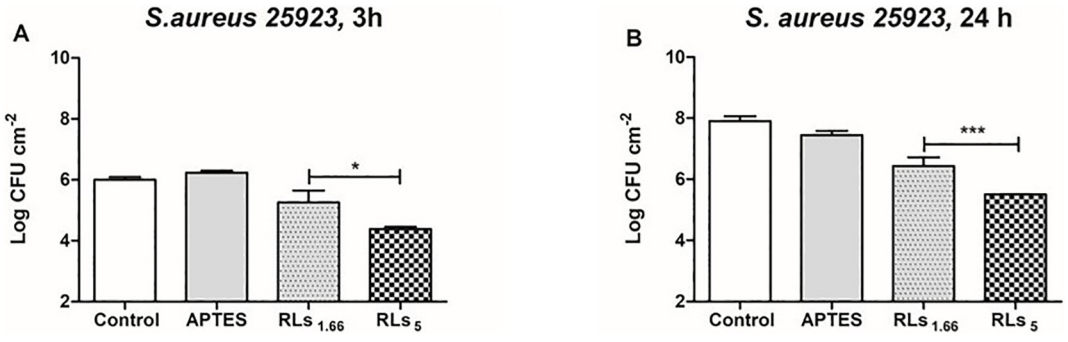

Fig. 2. *S. aureus* ATCC 25923 biofilm inhibition with $RLs_{1.66}$ and RLs_5 PDMS functionalized samples after 3 h (A) and 24 h (B) of incubation. (*$p < 0.05$, ***0.001).

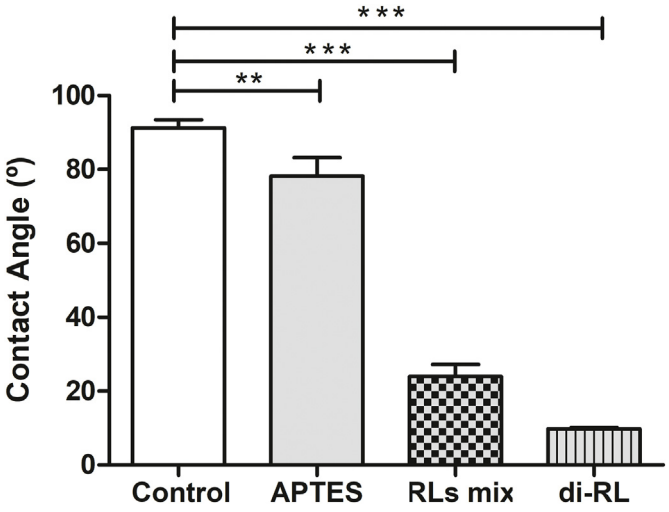

Fig. 3. Contact angle measurements (t = 10 min) of PDMS control and PDMS functionalized with APTES, RL*s* mixture (RL*s* mix) and RhaRhaC10C10:0 (di-RL). (**p < 0.01, ***0.001).

Contrary results were obtained by Hajfarajollah et al [40] but these authors used adsorption instead of chemical functionalization of the PDMS surface. In the mentioned study the results suggested that valleys may serve as anchoring or fling sites for the adsorption of other molecules.

3.3.1.3. Protein adsorption. When protein adsorption onto medical devices surface occurs that originates a layer favorable to bacteria adhesion and hence biofilm formation. The quantification of the BSA adsorbed on the PDMS control and RL*s*' functionalized PDMS surfaces was 0.075 ± 0.009 and 0.046 ± 0.012 mg cm^{-2}, respectively. Thus, when comparing to the medical grade silicone, a reduction of 38.7% in BSA adsorption was observed after RL*s* functionalization. This reduction might be attributed to the decrease in the surface hydrophobicity after RL*s* functionalization since hydrophobic interactions between the PDMS and proteins such as BSA have been reported by several authors [9,15].

3.4. Antibiofilm activity

Antibiofilm properties of RL*s* functionalized medical grade PDMS substrate was explored against *S. aureus* ATCC *25923*, *MRSA* and *S. epidermidis* ATCC 28319, which are representative bacteria of blood stream catheter related infections. Both RL*s* mix and di-RL functionalized samples, revealed a reduction on biofilm viability, reaching a decrease of

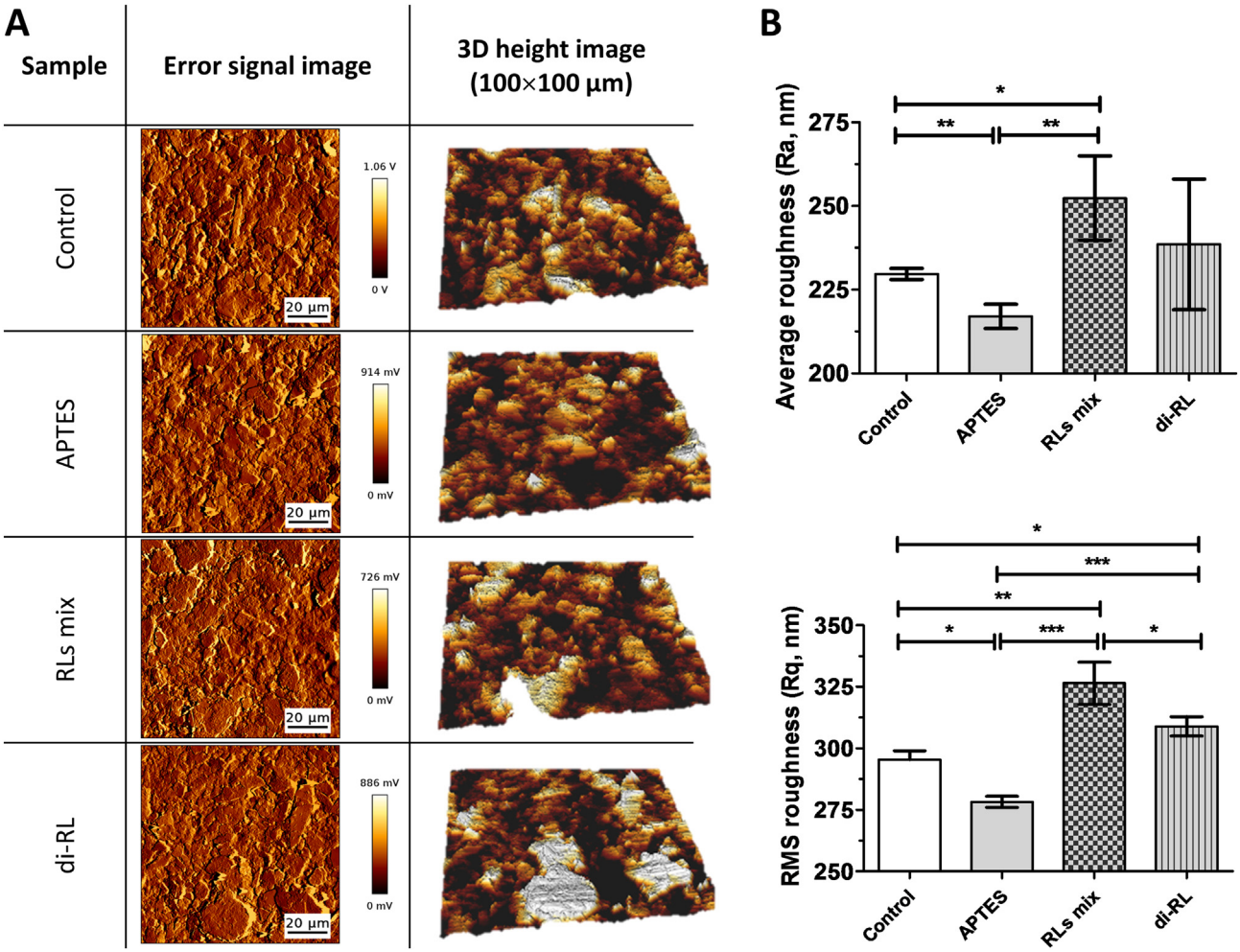

Fig. 4. A. Atomic force microscopy images of PDMS surfaces without functionalization and functionalized with APTES (APTES), with a mixture of RLs (RLs mix) or with isolated RL (di-RL). Height AFM images "3D image" (at a fixed scaled of 1 µm) and error signal image (100 µm × 100 µm). B. Analysis of AFM height images: average roughness (Ra) root and mean square roughness (RMS roughness, Rq) obtained for all the samples tested. Data is shown as mean value ± standard deviation (S·D). Statistical parameters: from Ra: *p = 0.0365 and **$p \leq$ 0.0095; and from Rq: *$p \leq$ 0.0328, **p = 0.0071 and ***$p \leq$ 0.0007.

2.4 and 2.3 Log (CFU cm^{-2}), respectively, when tested against *S. aureus 25923*. These results were significantly different when comparing to the control, (Fig. 5A and D). Regarding *MRSA* and *S. epidermidis* biofilm formation, 1 Log (CFU cm^{-2}) of reduction was observed and results were also significantly different when comparing to the control (Fig. 5B and C). However, no significant difference was observed when comparing APTES functionalized samples versus control samples, meaning that APTES functionalized samples did not have a considerable effect on biofilm inhibition regarding the different bacteria tested.

The CLSM biofilm observations allowed to verify the biofilm structure and the differentiation from live (green fluorescence) and dead (red fluorescence) bacteria. A dense and multi-layered biofilm architecture (green fluorescence) was observed on the plain PDMS substrates (used as positive controls) with all the used strains (Fig. $5A_1$-D_1). These multi-layered structures disappeared in RLs functionalized samples and dead bacteria could be observed in some specimens, leading to the observation that besides reducing adhesion to surfaces bacteria were also killed (Fig. $5A_2$-D_2).

To the best of our knowledge, this was the first time that RLs (i.e. as a mixture or isolated compounds) were covalently bonded to the PDMS surfaces for antibiofilm activity improvement. The results mentioned above revealed a synergy between the antimicrobial and the anti-adhesive properties of RLs making these compounds good candidates for the improvement of the medical devices antibiofilm properties.

Additionally, antibiofilm properties of isolated RLs have rarely been studied and most of the times were with a RLs-free solution added to a bacteria suspension or under a biofilm eradication approach [5]. For instance Aleksic et al. [24] reported that a Rha-RhaC10:0C10:0 (50 μg mL^{-1}) solution was able to inhibit *S. aureus* ATCC 25923 and MRSA biofilm formation up to 63 and 56%, while when under an eradication assay the same solution eradicated 57 and 58%, respectively. Moreover, most of biofilm studies have been performed with a rhamnolipids mixture. An example is presented in Shen et al. [5] studies that when using a RLs mixture solution (80 μg mL^{-1}) observed a *S. aureus* ATCC 25923 biofilm inhibition of 80% within 24 h. Under the scope of surface functionalization with these antimicrobial glycolipids adsorption approaches have been suggested. Ceresa et al. [21] found that RLs, produced by *P. aeruginosa* 89 (2 mg mL^{-1}), adsorbed to medical grade silicone, significantly reduced *S. aureus* ATCC 6538 and *S. epidermidis* ATCC 35984 biofilm formation by 76% and 63%, respectively, within 72 h. In addition, previous results from Rodrigues et al. [23] also exhibited the anti-adhesive capacity of the RLs when coating silicone rubber. When using a solution of 4 mg mL^{-1} to promote RLs adsorption, the number of the adhered bacteria (e.g. *S. aureus* and *S. epidermidis*) decreased to 48% after 4 h of incubation [23].

Two phenomena might contribute to the RLs antibiofilm effect, i.e. their anti-adhesive and antimicrobial properties [21,38]. Their anti-adhesive properties are closely related to the capacity of RLs to inverse the hydrophobic behavior of surfaces into hydrophilic making them unfavorable for hydrophobic bacteria adhesion [12]. In addition, the amphiphilic behavior of RLs molecules acting on cell-to-cell and cell-to-surface interactions may minimize the adherence capability of bacteria into the surface [43]. The observed decrease in contact angle measurements (Fig. 3) and in the initial bacteria adhesion (Fig. 2A) with RLs-functionalized samples are in accordance with the antiadhesive effect described for RLs. Moreover, the biocidal property of RLs manifested by their capability to disrupt and permeabilize the bacterial membrane was observed in surfaces where bacteria were stained by propidium iodide (Fig. 5). Findings suggest that RLs increase pore formation and disintegration of bacterial cell membrane [20,21,34]. For not presenting a specific antimicrobial molecular targeting mechanism RLs may be pointed out as antimicrobial molecules not likely to induce the development of resistance similarly to other membrane disturbing agents such as some antimicrobial peptides [44]. To conclude, RLs may stand for a good alternative to antibiotics with the additional advantage of avoiding the bacterial resistance phenomenon [20,21,34].

The obtained surfaces, for vascular catheters, showed distinctive antimicrobial properties against methicillin sensitive *S. aureus* ≈ 2.4 Log reduction. Although some authors have mentioned that in urinary catheters evidence of antimicrobial activity requires at least 3 log reduction in viability when compared to a control [45], currently there is no consensus on what log reduction is considered a suitable reduction for catheters. Different antiadhesive/antimicrobial strategies have been proposed to overcome catheter microbial colonization and in most cases reductions observed in the surface colonization range between 50 and 99% meaning that are decreases of 1–2 log units [3]. Among those approaches are hydrophilic coatings such as PEG-based, PEGMA brushes or natural polysaccharides grafting; zwitterionic polymers such as poly(betaines), amphiphilic polymers such as PEG-acrylate copolymers or heparin-mimetic polyurethanes; and micropatterned surfaces such as perfluorocarbon coatings or sharklet topography imprinted on PDMS [3].

3.5. Biocompatibility

3.5.1. In vitro cytocompatibility assessment

In order to provide a detailed evaluation of the in vitro biological response to the developed non and functionalized-PDMS samples, two different approaches were assessed using human dermal fibroblasts cultures: a direct assay (i.e. cells were seeded and grown directly over the materials) and an indirect assay (i.e. cells were seeded and grown in the same microenvironment of the materials, but without direct contact).

Regarding the direct assay, cultures grown over the culture plate presented a high metabolic activity at day 1, which increased significantly at day 5 (Fig. 6A). In contrast, cells grown directly over the non-functionalized-PDMS (control) and functionalized-PDMS (APTES, RLs mix, di-RL) samples presented a significantly decreased metabolic activity. At day 5, cultures grown on control conditions presented higher metabolic activity than those attained at day 1. Cultures grown on the surface of the distinct materials presented, comparatively, significant lower MTT reduction values, similar to those attained at day 1. This trend was confirmed by the fluorescence imaging of the human dermal fibroblasts (Fig. 6B). Regarding cells grown over the culture plate, a spread and stretched morphology was verified, with well-organized actin fibers distributed over the cytoplasm. Additionally, evident cytoplasmic extensions (filopodia) extending into significant intercellular contacts were attained, as well as a strong nucleus counter-staining. Cells grown over the non and functionalized-PDMS samples were rarely identified, presenting an altered and irregular morphology, as well as scattered cellular debris and remnants.

On the indirect assay, a distinct cellular behavior was attained. Controls presented a high metabolic activity at day 1, as well as the cultures grown in the presence of the developed materials, that presented high levels, despite the marginal reduction, as compared to control (Fig. 6). At day 5, the metabolic activity of control was found to increase around 2.5×, a trend also verified for the cultures grown in the presence of the non and functionalized-PDMS samples. Comparatively, the APTES and di-RL groups presented a significant higher metabolic activity in comparison to control and the other experimental groups. The cellular morphology of human dermal fibroblasts grown in the presence of the distinct developed materials was found to be quite similar to that of control, presenting similar morphological characteristics and intercellular contacts, of the fibroblastic phenotype (Fig. 7).

Overall, the direct assay revealed a trend for a reduced cell adhesion, as well as a limited metabolic activity and proliferative capability of the cultures grown on non and functionalized-PDMS samples. Contrariwise, the indirect assay revealed a high cellular adhesion and metabolic activity, fairly similar to the positive control. This behavior- impaired cell functionality in direct assays and adequate cell function in indirect testing- is in line with previous data of PDMS-based materials [46] and found to be adequate for the aimed biomedical application – i.e., vascular catheters. In these materials, cell adhesion and proliferation over the surface is not desirable - given the possible interference with the flow and/or activation of blood components, but simultaneously no adverse effects are intended for circulating or neighboring cells and tissues [47,48].

Given the aimed contact with blood, hemocompatibility assays were further conducted, regarding hemolysis (Fig. 8A) and platelet adhesion

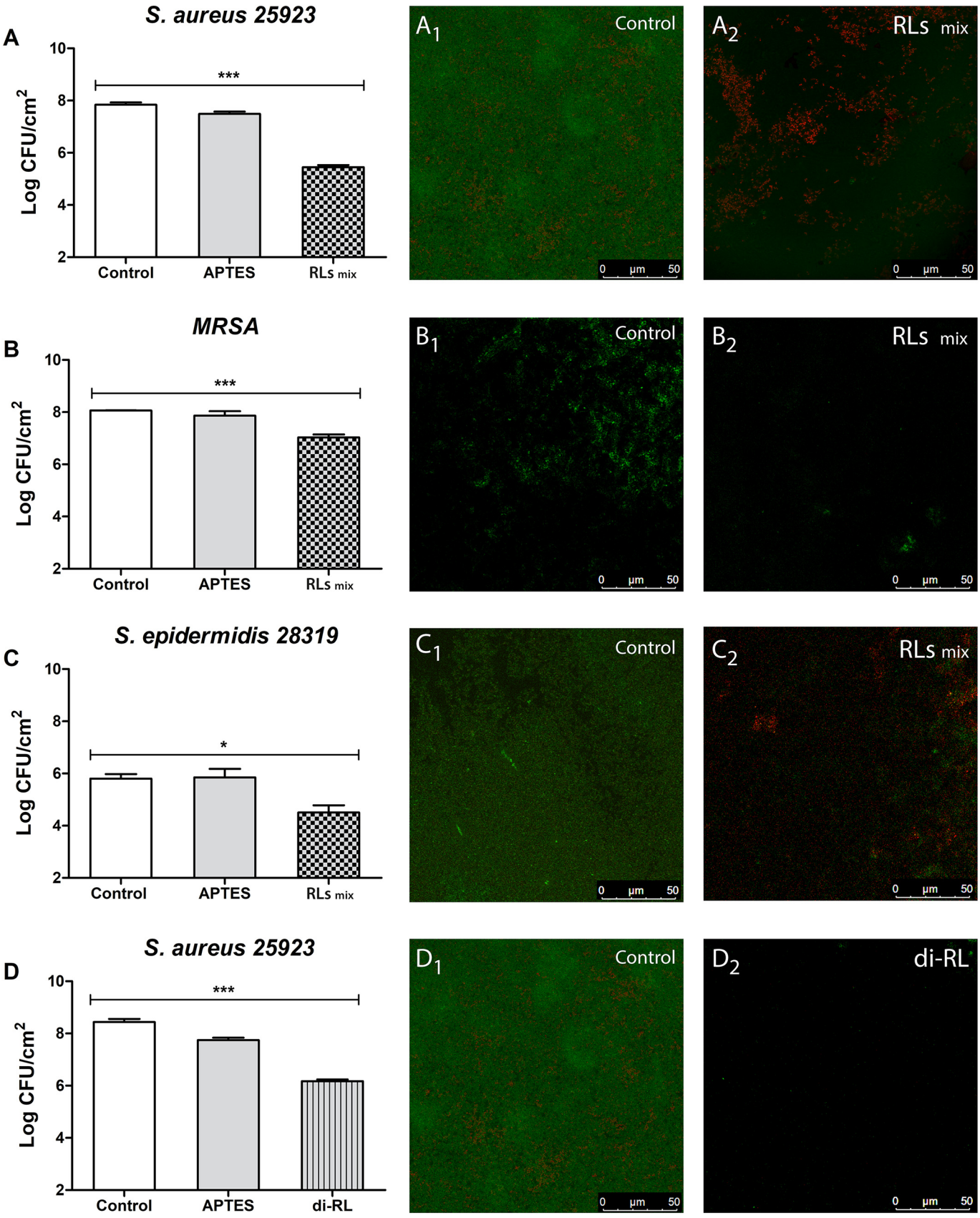

Fig. 5. Biofilm inhibition of RLs mix and di-RL surfaces against *S. aureus* ATCC *25923*, *MRSA and S. epidermidis* ATCC 28319 (*$p < 0.05$; ***0.001, statistically different from the control). Biofilm inhibition was assessed by colony forming unit counts (A-D). Confocal laser scanning microscopy allowed the visualization of controls (A_1-D_1) and functionalized samples surfaces (A_2-D_2).

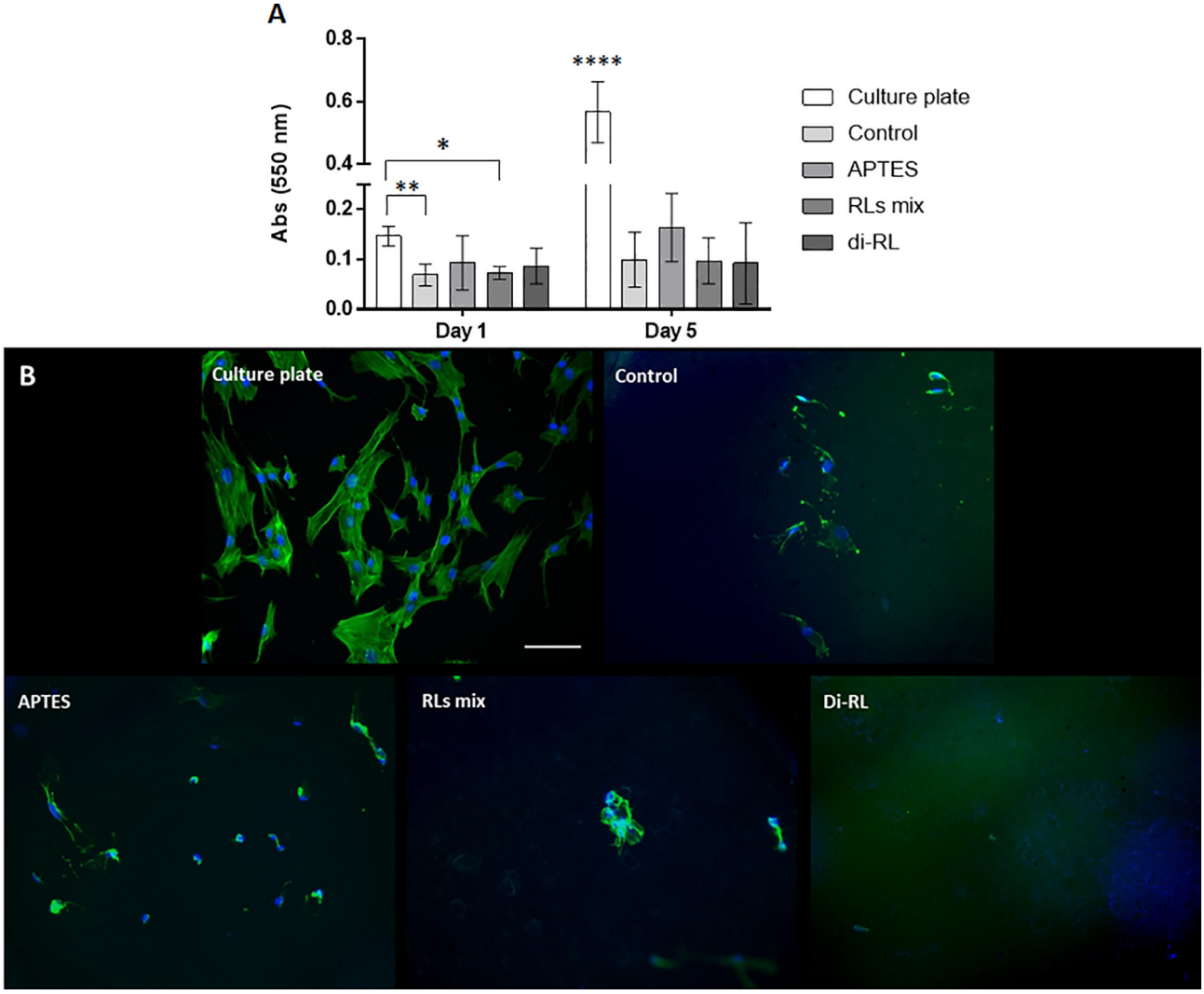

Fig. 6. Human dermal fibroblastic cell cultures grown directly over the membranes. A. Metabolic activity/Viability assay (MTT assay), at day 1 and 5. Statistical analysis, ANOVA followed by Tuckey's test, $n = 5$, $^{*}p < 0.05$, **0.01; ****0.0001, between culture plate and the remaining conditions. B. Representative fluorescence images of human dermal fibroblasts, at day 1, stained for actin cytoskeleton in green and counter-stained for the nucleus in blue. Scale bar corresponds to 100 μm. Control: bare PDMS.

(Fig. 8B). Regarding the hemolysis assay, a comparative analysis revealed no significant differences between PMDS and di-RL samples, which presented a very low hemolysis rate - lower than 1.5% and 1.6%, respectively. RLs mix group presented a slightly higher hemolysis rate, of around 3.5%, being however significantly lower than the critical threshold of 5%, established by the ASTM F756 standards, for materials with the potential capacity to induce hemolysis (ASTM, 2017). In addition to the hemolysis assessment, platelet adhesion assays were conducted by SEM imaging. Platelets adhered to the negative control presented a broadly round/discoid morphology, similar to the one attained in those adhered to RLs mix samples. Platelets adhered to Control and di-RL presented minor spreading and minimal extension of pseudopodia. Adherent platelet morphology can be classified into five categories, according to the progressive degree of activation: round/discoid, with the absence of pseudopodia; dendritic or early pseudopodial, with minor peusopodia and absence of flattening; spread dendritic or intermediate pseudopodial, evidencing at least one flattened pseudopodia and the absence of hyaloplasma spreading between pseudopodia; spreading, with the spreading of hyaloplasma between pseudopodia and fully spread, with a generalized hyaloplasma spreading and indistinguishable pseudopodia organization [49]. Overall, a general trend to limit platelet activation was verified in all PDMS surfaces, by the absence of identifiable dendritic or spread morphologic features. Attained data is in accordance with the reported adequacy of PDMS functionality regarding platelet function, showcasing the ability of this material to lessen platelet adhesion and activation, as compared to other reference materials [46,50,51]. These properties do not seem to be broadly modified by the functionalization with either the isolated di-RL or RLs mix, with the later further promoting the maintenance of the round morphology.

3.5.2. Vascular irritation assessment

The vascular irritation potential of the developed membranes was assessed by the HET-CAM test. As observed in Fig. 9, the positive control (NaOH) induced fast and progressive vascular alterations, characterized by lysis, hemorrhage and coagulation, further increasing in intensity with time. The negative control (NaCl), as well as all experimental groups, induced no significant vascular alterations throughout the assay period (5 min), being characterized as non-irritating substrates. In accordance, PDMS has been established not to induce irritation or sensitization to experimental animals or humans, upon direct exposure [52]. Further, RLs were found to induce no irritation on comparable ocular and skin irritation assays [53,54], supporting the use of the developed PDMS-based materials in biomedical applications.

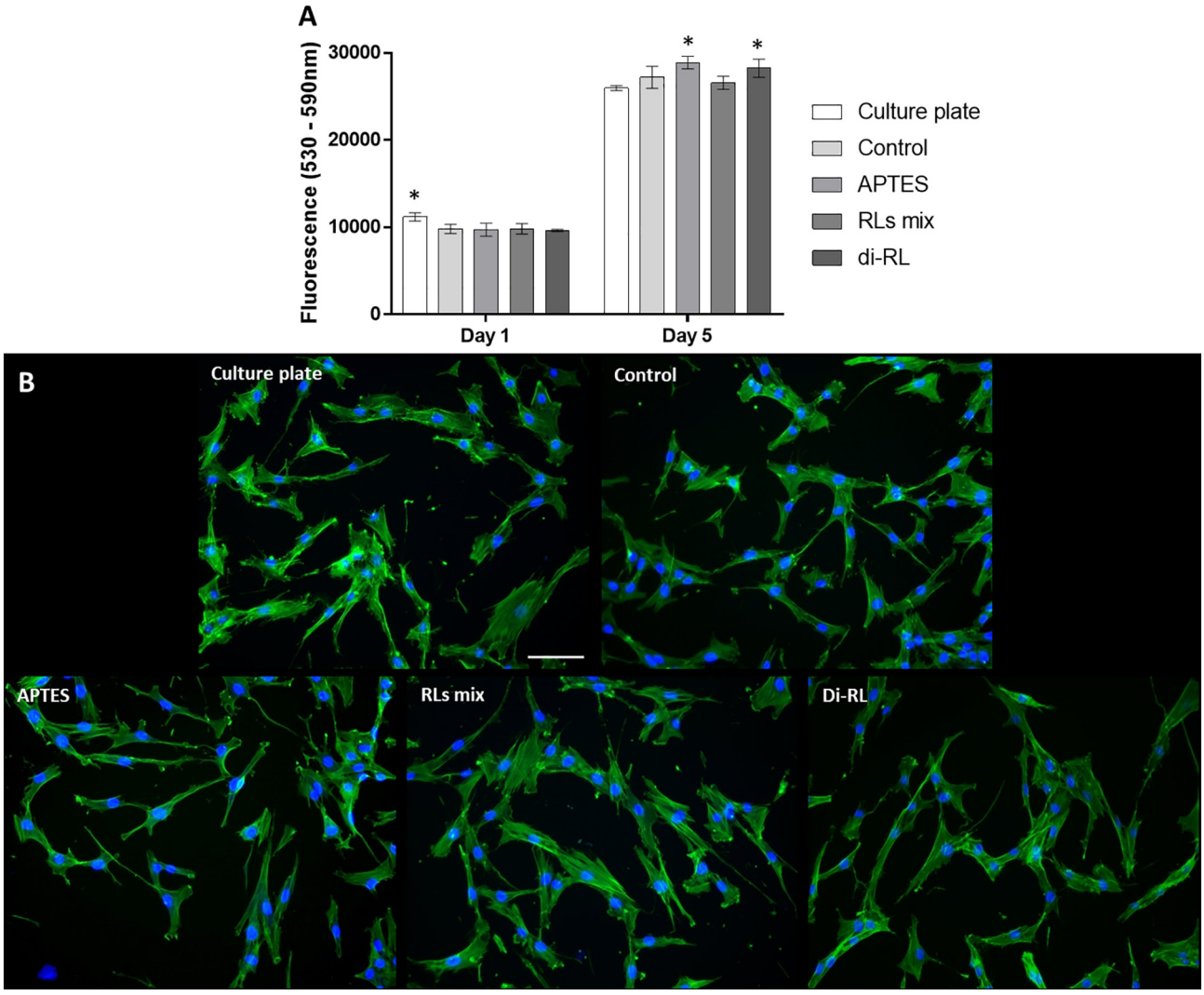

Fig. 7. Human dermal fibroblastic cell cultures grown with indirect contact with the membranes, through a permeable culture insert. A. Metabolic activity/Viability assay (Resazurin fluorescence), at day 1 and 5. Statistical analysis, ANOVA followed by Tuckey's test, $n = 5$, $^*p < 0.05$ vs the remaining conditions. B. Representative fluorescence images of human dermal fibroblasts morphology, at day 1, stained for actin cytoskeleton in green and counter-stained for the nucleus in blue. Scale bar corresponds to 100 μm. Control: bare PDMS.

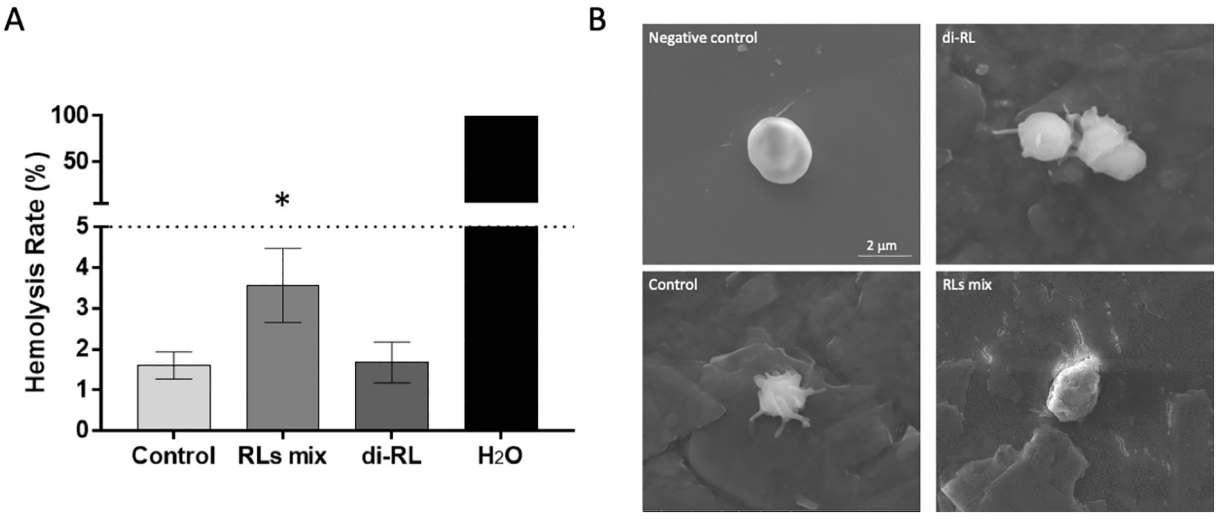

Fig. 8. Hemocompatibility assessment of the developed materials. A. Hemolysis assay: Positive control (distilled water, H_2O) was set as 100% of hemolysis, while the negative control (NaCl 0.9%) was set as 0%. Statistical analysis, ANOVA followed by Tuckey's test, $n = 5$, $^*p < 0.05$ vs the remaining conditions. *Statistically different from Control and di-RL. B. Platelet activation assay. Representative SEM images of adhered platelets.

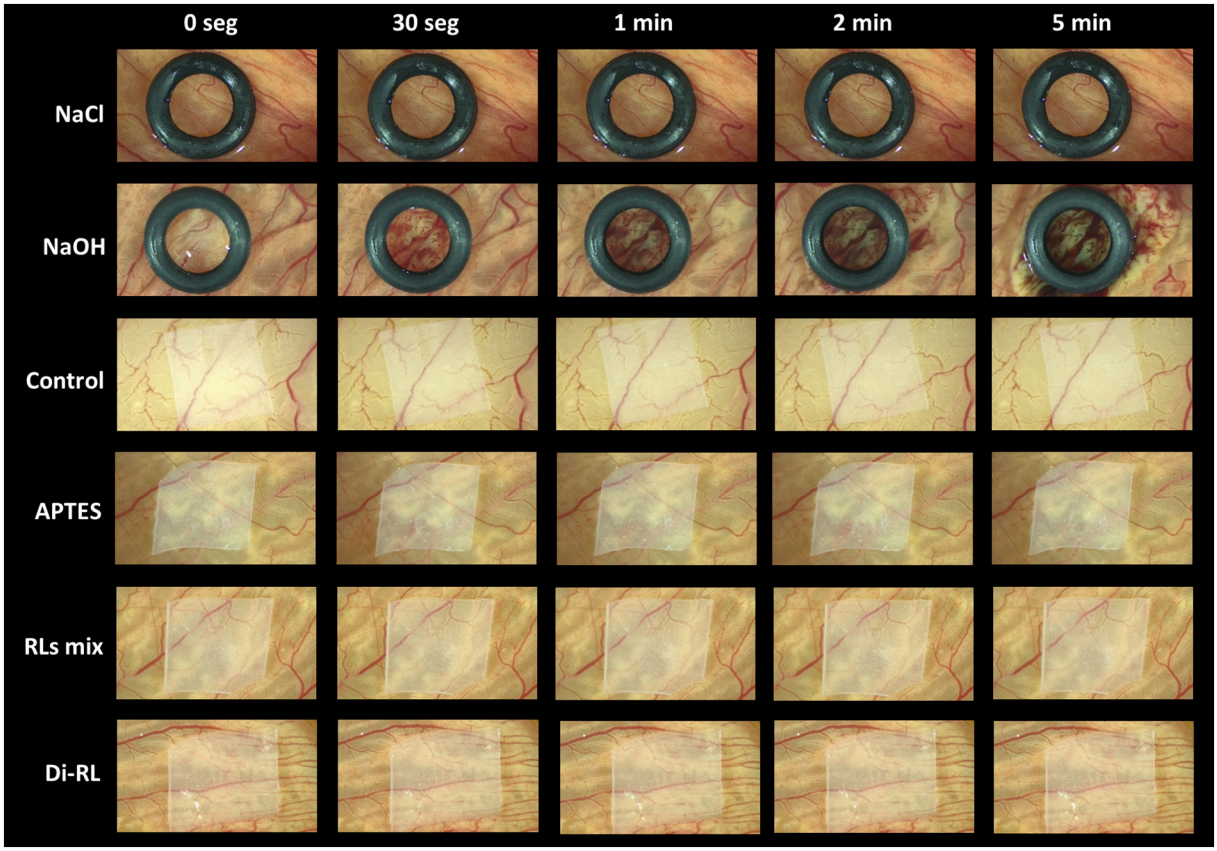

Fig. 9. Vascular irritation Het-CAM assay. Representative *in ovo* CAM images of the non and functionalized-PDMS samples, positive control (NaOH) and negative control (NaCl) up to the 5 min endpoint.

4. Conclusions

In this work we hypothesized that by functionalizing silicone surface with rhamnolipids biosurfactants the antimicrobial properties of medical grade PDMS could be improved. Rhamnolipids were successfully grafted onto PDMS surface by covalent bond after plasma activation and APTES anchoring. This functionalization allowed a longer lasting approach that enhanced PDMS antimicrobial properties being an advantage when compared to other approaches such as adsorption commonly mentioned in literature. Surfaces become more hydrophilic and rougher and were able to reduce Gram-positive bacteria colonization and biofilm formation. Biocompatibility of functionalized samples was confirmed in different ways, namely, by cell viability, hemocompatibility and vascular irritation assessment. Moreover, a purified and single RL (i.e. RhaRhaC10C10:0) was for the first time covalently bonded to PDMS surface and not only proved to have antibiofilm activity but also to be biocompatible which may become an advantage considering medical field applications that use this biomaterial and want to improve its antimicrobial properties.

CRediT authorship contribution statement

M. Dardouri: Investigation, Methodology, Original draft preparation. **A. Bettencourt**: Writing-Original draft. **V. Martin**: Investigation, Methodology. **F.A. Carvalho**: Investigation, Methodology, Writing-Original draft. **C. Santos**: Validation. **N. Monge**: Visualization. **N.C. Santos**: Resources, Writing-review. **M.H. Fernandes**: Resources. **P.S. Gomes**: Conceptualization, Supervision, Writing-Original draft, Writing-review & editing. **I.A.C. Ribeiro**: Conceptualization, Supervision, Writing-Original draft, Writing-review & editing, Project administration, Resources, Funding acquisition.

Declaration of competing interest

The authors declare that they have no known competing financial interests or personal relationships that could have appeared to influence the work reported in this paper.

Acknowledgements

The authors thank Fundação para a Ciência e Tecnologia (FCT) for the financial support under Project PTDC/BTM-SAL/29335/2017. The authors would also like to acknowledge Portuguese Mass Spectrometry Network (Rede Nacional de Espectrometria de Massa RNEM). The authors also acknowledge Andreia Bento for the assistance with the UHPLC-MS/MS equipment and Professor Maria José Umbelino for allowing the use of the automatic flash chromatography system. The authors gratefully acknowledge Biosurfit company for providing the plasma equipment.

References

[1] Z. Zhu, Z. Wang, S. Li, X. Yuan, Antimicrobial strategies for urinary catheters, J. Biomed. Mater. Res. A 107 (2019) 445–467, https://doi.org/10.1002/jbm.a.36561.
[2] S.I.C. Ricardo, I.I.L. Anjos, N. Monge, C.M.C. Faustino, I.A.C. Ribeiro, A glance at antimicrobial strategies to prevent catheter-associated medical infections, ACS Infect. Dis. 6 (2020) 3109–3130, https://doi.org/10.1021/acsinfecdis.0c00526.
[3] C.M.C. Faustino, S.M.C. Lemos, N. Monge, I.A.C. Ribeiro, A scope at antifouling strategies to prevent catheter-associated infections, Adv. Colloid Interf. Sci. 284 (2020), 102230, https://doi.org/10.1016/j.cis.2020.102230.
[4] S. Zhang, J. Vaida, J. Parenti, B.A. Lindsey, M. Xing, B. Li, Programmed multidrug delivery based on bio-inspired capsule-integrated nanocoatings for infected bone defect treatment, ACS Appl. Mater. Interfaces 13 (2021) 12454–12462, https://doi.org/10.1021/acsami.0c20332.

[5] Y. Shen, P. Li, X. Chen, Y. Zou, H. Li, G. Yuan, H. Hu, Activity of sodium lauryl sulfate, rhamnolipids, and N-acetylcysteine against biofilms of five common pathogens, Microb. Drug Resist. 26 (2020) 290–299, https://doi.org/10.1089/mdr.2018.0385.

[6] J.D.P. Valentin, X.-H. Qin, C. Fessele, H. Straub, H.C. van der Mei, M.T. Buhmann, K. Maniura-Weber, Q. Ren, Substrate viscosity plays an important role in bacterial adhesion under fluid flow, J. Colloid Interface Sci. 552 (2019) 247–257, https://doi.org/10.1016/j.jcis.2019.05.043.

[7] S. Kuddannaya, J. Bao, Y. Zhang, Enhanced in vitro biocompatibility of chemically modified Poly(dimethylsiloxane) surfaces for stable adhesion and long-term investigation of brain cerebral cortex cells, ACS Appl. Mater. Interfaces 7 (2015) 25529–25538, https://doi.org/10.1021/acsami.5b09032.

[8] R. Wang, K.G. Neoh, E.-T. Kang, Integration of antifouling and bactericidal moieties for optimizing the efficacy of antibacterial coatings, J. Colloid Interface Sci. 438 (2015) 138–148, https://doi.org/10.1016/j.jcis.2014.09.070.

[9] M.S. Birajdar, B.H. Kim, C. Sutthiwanjampa, S.H. Kang, C.Y. Heo, H. Park, Inhibition of capsular contracture of poly (Dimethyl Siloxane) medical implants by surface modification with itaconic acid conjugated gelatin, J. Ind. Eng. Chem. 89 (2020) 128–138, https://doi.org/10.1016/j.jiec.2020.03.036.

[10] A. Köllnberger, R. Schrader, C.A. Briehn, Carboxylic acid mediated antimicrobial activity of silicone elastomers, Mater. Sci. Eng. C. 113 (2020), 111001, https://doi.org/10.1016/j.msec.2020.111001.

[11] S. Ghamrawi, J.-P. Bouchara, O. Tarasyuk, S. Rogalsky, L. Lyoshina, O. Bulko, J.-F. Bardeau, Promising silicones modified with cationic biocides for the development of antimicrobial medical devices, Mater. Sci. Eng. C. 75 (2017) 969–979, https://doi.org/10.1016/j.msec.2017.03.013.

[12] M. Lam, V. Migonney, C. Falentin-Daudre, Review of silicone surface modification techniques and coatings for antibacterial/antimicrobial applications to improve breast implant surfaces, Acta Biomater. 121 (2021) 68–88, https://doi.org/10.1016/j.actbio.2020.11.020.

[13] M.M. Sugii, F.A.de S. Ferreira, K.C. Müller, D.A.N.L. Lima, F.C. Groppo, H. Imasato, U.P. Rodrigues-Filho, F.H.B. Aguiar, Physical, chemical and antimicrobial evaluation of a composite material containing quaternary ammonium salt for braces cementation, Mater. Sci. Eng. C 73 (2017) 340–346, https://doi.org/10.1016/j.msec.2016.12.084.

[14] S. Zanini, A. Polissi, E.A. Maccagni, E.C. Dell'Orto, C. Liberatore, C. Riccardi, Development of antibacterial quaternary ammonium silane coatings on polyurethane catheters, J. Colloid Interface Sci. 451 (2015) 78–84, https://doi.org/10.1016/j.jcis.2015.04.007.

[15] Z. Li, X. Yang, H. Liu, X. Yang, Y. Shan, X. Xu, S. Shang, Z. Song, Dual-functional antimicrobial coating based on a quaternary ammonium salt from rosin acid with in vitro and in vivo antimicrobial and antifouling properties, Chem. Eng. J. 374 (2019) 564–575, https://doi.org/10.1016/j.cej.2019.05.208.

[16] H. Shahrour, I. Dandache, A.L. Martínez-López, G. González-Gaitano, A. Chokr, G. Martínez-de-Tejada, An antibiotic potentiator retains its activity after being immobilized on silicone and prevents growth of multidrug-resistant Pseudomonas aeruginosa biofilms, Mater. Sci. Eng. C. 121 (2021), 111876, https://doi.org/10.1016/j.msec.2021.111876.

[17] R. Mishra, A.K. Panda, S. De Mandal, M. Shakeel, S.S. Bisht, J. Khan, Natural antibiofilm agents: strategies to control biofilm-forming pathogens, Front. Microbiol. 11 (2020), https://doi.org/10.3389/fmicb.2020.566325.

[18] C. Ceresa, M. Rinaldi, F. Tessarolo, D. Maniglio, E. Fedeli, E. Tambone, P. Caciagli, I.M. Banat, M.A. Diaz De Rienzo, L. Fracchia, Inhibitory effects of lipopeptides and glycolipids on C. albicans–Staphylococcus spp. dual-species biofilms, Front. Microbiol. 11 (2021) 1–19, https://doi.org/10.3389/fmicb.2020.545654.

[19] P. Palanisamy, A.M. Raichur, Synthesis of spherical NiO nanoparticles through a novel biosurfactant mediated emulsion technique, Mater. Sci. Eng. C. 29 (2009) 199–204, https://doi.org/10.1016/j.msec.2008.06.008.

[20] V.K. Gaur, V. Tripathi, P. Gupta, N. Dhiman, R.K. Regar, K. Gautam, J.K. Srivastava, S. Patnaik, D.K. Patel, N. Manickam, Rhamnolipids from planococcus spp. And their mechanism of action against pathogenic bacteria, Bioresour. Technol. 307 (2020), 123206, https://doi.org/10.1016/j.biortech.2020.123206.

[21] C. Ceresa, F. Tessarolo, D. Maniglio, E. Tambone, I. Carmagnola, E. Fedeli, I. Caola, G. Nollo, V. Chiono, G. Allegrone, M. Rinaldi, L. Fracchia, Medical-grade silicone coated with rhamnolipid R89 is effective against staphylococcus spp. biofilms, Molecules 24 (2019), https://doi.org/10.3390/molecules24213843.

[22] A. Chebbi, M. Elshikh, F. Haque, S. Ahmed, S. Dobbin, R. Marchant, S. Sayadi, M. Chamkha, I.M. Banat, Rhamnolipids from Pseudomonas aeruginosa strain W10; as antibiofilm/antibiofouling products for metal protection, J. Basic Microbiol. 57 (2017) 364–375, https://doi.org/10.1002/jobm.201600658.

[23] L.R. Rodrigues, I.M. Banat, H.C. Van Der Mei, J.A. Teixeira, R. Oliveira, Interference in adhesion of bacteria and yeasts isolated from explanted voice prostheses to silicone rubber by rhamnolipid biosurfactants, J. Appl. Microbiol. 100 (2006) 470–480, https://doi.org/10.1111/j.1365-2672.2005.02826.x.

[24] I. Aleksic, M. Petkovic, M. Jovanovic, D. Milivojevic, B. Vasiljevic, J. Nikodinovic-Runic, L. Senerovic, Anti-biofilm properties of bacterial Di-rhamnolipids and their semi-synthetic amide derivatives, Front. Microbiol. 8 (2017) 1–16, https://doi.org/10.3389/fmicb.2017.02454.

[25] M. Dardouri, R.M. Mendes, J. Frenzel, J. Costa, I.A.C. Ribeiro, Seeking faster, alternative methods for glycolipid biosurfactant characterization and purification, Anal. Bioanal. Chem. 413 (2021) 4311–4320, https://doi.org/10.1007/s00216-021-03387-4.

[26] R.M. Mendes, A.P. Francisco, F.A. Carvalho, M. Dardouri, B. Costa, A.F. Bettencourt, J. Costa, L. Gonçalves, F. Costa, I.A.C. Ribeiro, Fighting S. aureus catheter-related infections with sophorolipids: electing an antiadhesive strategy or a release one? Colloids Surf. B: Biointerfaces 208 (2021), 112057, https://doi.org/10.1016/j.colsurfb.2021.112057.

[27] A. Ascenso, M. Cruz, C. Euletério, F.A. Carvalho, N.C. Santos, H.C. Marques, S. Simões, Novel tretinoin formulations: a drug-in-cyclodextrin-in-liposome approach, J. Liposome Res. 23 (2013) 211–219, https://doi.org/10.3109/08982104.2013.788026.

[28] F.A. Carvalho, S. Connell, G. Miltenberger-Miltenyi, S.V. Pereira, A. Tavares, R.A.S. Ariëns, N.C. Santos, Atomic force microscopy-based molecular recognition of a fibrinogen receptor on human erythrocytes, ACS Nano 4 (2010) 4609–4620, https://doi.org/10.1021/nn1009648.

[29] G. Mancini, L.M.D. Gonçalves, J. Marto, F.A. Carvalho, S. Simões, H.M. Ribeiro, A.J. Almeida, Increased therapeutic efficacy of SLN containing etofenamate and ibuprofen in topical treatment of inflammation, Pharmaceutics 13 (2021) 328, https://doi.org/10.3390/pharmaceutics13030328.

[30] Bio-Rad Laboratories, Bio-Rad Protein Assay (Bradford), Bio-Rad 2010, pp. 1–24.

[31] C. Pontes, M. Alves, C. Santos, M.H. Ribeiro, L. Gonçalves, A.F. Bettencourt, I.A.C. Ribeiro, Can sophorolipids prevent biofilm formation on silicone catheter tubes? Int. J. Pharm. 513 (2016) 697–708, https://doi.org/10.1016/j.ijpharm.2016.09.074.

[32] C. Severo, I. Anjos, V.G.L. Souza, J.P. Canejo, M.R. Bronze, A.L. Fernando, I. Coelhoso, A.F. Bettencourt, I.A.C. Ribeiro, Development of cranberry extract films for the enhancement of food packaging antimicrobial properties, Food Packag. Shelf Life 28 (2021), 100646, https://doi.org/10.1016/j.fpsl.2021.100646.

[33] M. Ferreira, O. Rzhepishevska, L. Grenho, D. Malheiros, L. Gonçalves, A.J. Almeida, L. Jordão, I.A. Ribeiro, M. Ramstedt, P. Gomes, A. Bettencourt, Levofloxacin-loaded bone cement delivery system: highly effective against intracellular bacteria and Staphylococcus aureus biofilms, Int. J. Pharm. 532 (2017) 241–248, https://doi.org/10.1016/j.ijpharm.2017.08.089.

[34] A.M. Abdel-Mawgoud, F. Lépine, E. Déziel, Rhamnolipids: diversity of structures, microbial origins and roles, Appl. Microbiol. Biotechnol. 86 (2010) 1323–1336, https://doi.org/10.1007/s00253-010-2498-2.

[35] M. Elshikh, I. Moya-Ramírez, H. Moens, S. Roelants, W. Soetaert, R. Marchant, I.M. Banat, Rhamnolipids and lactonic sophorolipids: natural antimicrobial surfactants for oral hygiene, J. Appl. Microbiol. 123 (2017) 1111–1123, https://doi.org/10.1111/jam.13550.

[36] A.M. Ferreira, I. Carmagnola, V. Chiono, P. Gentile, L. Fracchia, C. Ceresa, G. Georgiev, G. Ciardelli, Surface modification of poly(dimethylsiloxane) by two-step plasma treatment for further grafting with chitosan-rose Bengal photosensitizer, Surf. Coat. Technol. 223 (2013) 92–97, https://doi.org/10.1016/j.surfcoat.2013.02.035.

[37] X. Shi, Y. Chen, X. Zhang, X. Long, J. Qian, Biomass rhamnolipid modified poly(vinylidene fluoride) membrane with significantly improved surface hydrophilicity and enhanced antifouling performance, Chem. Eng. Sci. 212 (2020), 115330, https://doi.org/10.1016/j.ces.2019.115330.

[38] A.F. Bettencourt, C. Tomé, T. Oliveira, V. Martin, C. Santos, L. Gonçalves, M.H. Fernandes, P.S. Gomes, I.A.C. Ribeiro, Exploring the potential of chitosan-based particles as delivery-carriers for promising antimicrobial glycolipid biosurfactants, Carbohydr. Polym. 254 (2020), 117433, https://doi.org/10.1016/j.carbpol.2020.117433.

[39] T.A.A. Moussa, M.S. Mohamed, N. Samak, Production and characterization of di-rhamnolipid produced by Pseudomonas aeruginosa TMN, Braz. J. Chem. Eng. 31 (2014) 867–880, https://doi.org/10.1590/0104-6632.20140314s00002473.

[40] H. Hajfarajollah, S. Mehvari, M. Habibian, B. Mokhtarani, K.A. Noghabi, Rhamnolipid biosurfactant adsorption on a plasma-treated polypropylene surface to induce antimicrobial and antiadhesive properties, RSC Adv. 5 (2015) 33089–33097, https://doi.org/10.1039/c5ra01233c.

[41] J.A. Juárez-Moreno, A. Ávila-Ortega, A.I. Oliva, F. Avilés, J.V. Cauich-Rodríguez, Effect of wettability and surface roughness on the adhesion properties of collagen on PDMS films treated by capacitively coupled oxygen plasma, Appl. Surf. Sci. 349 (2015) 763–773, https://doi.org/10.1016/j.apsusc.2015.05.063.

[42] F. Poncin-Epaillard, J.M. Herry, P. Marmey, G. Legeay, D. Debarnot, M.N. Bellon-Fontaine, Elaboration of highly hydrophobic polymeric surface — a potential strategy to reduce the adhesion of pathogenic bacteria? Mater. Sci. Eng. C. 33 (2013) 1152–1161, https://doi.org/10.1016/j.msec.2012.12.020.

[43] A. Nickzad, E. Déziel, The involvement of rhamnolipids in microbial cell adhesion and biofilm development - an approach for control? Lett. Appl. Microbiol. 58 (2014) 447–453, https://doi.org/10.1111/lam.12211.

[44] J. Lei, L.C. Sun, S. Huang, C. Zhu, P. Li, J. He, V. Mackey, D.H. Coy, Q.Y. He, The antimicrobial peptides and their potential clinical applications, Am. J. Transl. Res. 11 (2019) 3919–3931.

[45] M. Ramstedt, I.A.C. Ribeiro, H. Bujdakova, F.J.M. Mergulhão, L. Jordao, P. Thomsen, M. Alm, M. Burmølle, T. Vladkova, F. Can, M. Reches, M. Riool, A. Barros, R.L. Reis, E. Meaurio, J. Kikhney, A. Moter, S.A.J. Zaat, J. Sjollema, Evaluating efficacy of antimicrobial and antifouling materials for urinary tract medical devices: challenges and recommendations, Macromol. Biosci. 19 (2019) 1–26, https://doi.org/10.1002/mabi.201800384.

[46] M.-C. Bélanger, Y. Marois, Hemocompatibility, biocompatibility, inflammatory and in vivo studies of primary reference materials low-density polyethylene and polydimethylsiloxane: a review, J. Biomed. Mater. Res. 58 (2001) 467–477, https://doi.org/10.1002/jbm.1043.

[47] Q. Tian, M. Deo, L. Rivera-Castaneda, H. Liu, Cytocompatibility of magnesium alloys with human urothelial cells: a comparison of three culture methodologies, ACS Biomater. Sci. Eng. 2 (2016) 1559–1571, https://doi.org/10.1021/acsbiomaterials.6b00325.

[48] D. Kowalczuk, A. Przekora, G. Ginalska, Biological safety evaluation of the modified urinary catheter, Mater. Sci. Eng. C. 49 (2015) 274–280, https://doi.org/10.1016/j.msec.2015.01.001.

[49] S.L. Goodman, Sheep, pig, and human platelet-material interactions with model cardiovascular biomaterials, J. Biomed. Mater. Res. 45 (1999) 240–250, https://doi.org/10.1002/(SICI)1097-4636(19990605)45:3<240::AID-JBM12>3.0.CO;2-C.

[50] M. Dabagh, M.J. Abdekhodaie, M.T. Khorasani, Effects of polydimethylsiloxane grafting on the calcification, physical properties, and biocompatibility of polyurethane in a heart valve, J. Appl. Polym. Sci. 98 (2005) 758–766, https://doi.org/10.1002/app.22132.

[51] E.M. Keough, W.C. Mackey, R. Connolly, T. Foxall, K. Ramberg-Laskaris, J.L. McCullough, T.F. O'Donnell, A.D. Callow, The interaction of blood components with PDMS(polydimethylsiloxane) and LDPE (low-density polyethylene) in a baboonex vivo arteriovenous shunt model, J. Biomed. Mater. Res. 19 (1985) 577–587, https://doi.org/10.1002/jbm.820190509.
[52] ECETOC, Environmental Impact Assessment for Socio-EConomic Analysis of Chemicals: Principles and Practice, 113, 2011, p. 82.
[53] E. Haba, A. Pinazo, O. Jauregui, M.J. Espuny, M.R. Infante, A. Manresa, Physicochemical characterization and antimicrobial properties of rhamnolipids produced byPseudomonas aeruginosa 47T2 NCBIM 40044, Biotechnol. Bioeng. 81 (2003) 316–322, https://doi.org/10.1002/bit.10474.
[54] P. Bharali, S. Das, A. Ray, S. Pradeep Singh, U. Bora, B. Kumar Konwar, C.B. Singh, D. Sahoo, Biocompatibility natural effect of rhamnolipids in bioremediation process on different biological systems at the site of contamination, Bioremediat. J. 22 (2018) 91–102, https://doi.org/10.1080/10889868.2018.1516616.